

LEIDEN UNIVERSITY

MASTERS THESIS

Design and Demonstration of Focal Plane Wavefront sensing for co-phasing the GMT

Author:
Alex Tripsas

Supervisor:
Dr. Kelsey Miller
& Prof. Matthew Kenworthy
& MSc. Steven Bos

*A thesis submitted in fulfillment of the requirements
for the degree of Masters Thesis*

in the department for
Astronomy and Instrumentation

July 1, 2020

Declaration of Authorship

I, Alex Tripsas, declare that this thesis titled, "Design and Demonstration of Focal Plane Wavefront sensing for co-phasing the GMT" and the work presented in it are my own. I confirm that:

- This work was done wholly or mainly while in candidature for a research degree at this University.
- Where any part of this thesis has previously been submitted for a degree or any other qualification at this University or any other institution, this has been clearly stated.
- Where I have consulted the published work of others, this is always clearly attributed.
- Where I have quoted from the work of others, the source is always given. With the exception of such quotations, this thesis is entirely my own work.
- I have acknowledged all main sources of help.
- Where the thesis is based on work done by myself jointly with others, I have made clear exactly what was done by others and what I have contributed myself.

Signed:

Date:

*"Now is the moment that everything can change
You are completely responsible for your own life
And no one is coming to save you from yourself
So stop blaming your problems on any or everything else
It does not matter one tiny fucking bit
How unfair you think the world is
It's only what you do
Right here, right now
Right this fucking instant that matters
It's your choice to
Sink or swim"*

D. Randall Blythe

LEIDEN UNIVERSITY

Abstract

Astronomy Department
Astronomy and Instrumentation

Masters Thesis

**Design and Demonstration of Focal Plane Wavefront sensing for co-phasing the
GMT**

by Alex Tripsas

The 25 meter, Giant Magellan Telescope (GMT) will be comprised of seven 8.4 meter mirrors that will have a resolving power ten times greater than that of the Hubble Space Telescope. The GMT will be capable of directly imaging nearby exoplanets with an angular resolution of 10-30 milliarcseconds in the near-IR. To make this possible, the seven separate mirrors need to be co-phased to a fraction of a wavelength to act as one 25 meter aperture. To co-phase the mirrors, we propose to use an Asymmetric Pupil vector Apodizing Phase Plate (APvAPP). The APvAPP generates two science images which can be used to sense aberrations in the pupil. This focal-plane wavefront sensing (FPWFS) technique will allow for the determination of segment piston, tip, and tilt. For simulation work, the python software package HCIPy was used to optimize the asymmetry of the APvAPP. Simulations are verified in the laboratory with a low-order deformable mirror (DM) to induce and then correct wavefront errors into a liquid crystal APvAPP located in a conjugate pupil plane. Here we present results of the development, optimization, and testing of the APvAPP in the laboratory.

Acknowledgements

I'd like to thank Dr. Kelsey Miller
Steven Bos

To all my old colleagues back at University of California Santa Cruz for, despite me not being there anymore, to continue to help me. Notably, Will Deich, if it weren't for you, this research would have been a nightmare.

Lastly, Professor Matthew Kenworthy

Contents

Declaration of Authorship	iii
Abstract	vii
Acknowledgements	ix
1 Introduction	1
1.1 Segmented Mirrors / Active Optics	2
1.2 FPWFS	4
1.2.1 Vector Apodizing Phase Plate	4
1.2.2 Asymmetric Pupil	5
2 Simulation	7
2.1 Response Matrix	7
2.2 Control Matrix	10
3 Optical Testbed	13
3.1 Optical Layout	13
3.2 Optical Alignment	14
3.3 Images & Wavefront Decomposition	16
4 Results	19
4.1 Simulation Results	19
4.2 Testbed Results	21
4.3 Future Work	21
A Response Matrix Images	23
B Simulation Results	25

List of Figures

1.1	Image of the Hale 200-inch (5.1m) primary mirror. The honeycomb structure was to reduce the mass of the optic and make the surface more ridged	1
1.2	Jerry Nelson showing his segmented mirror design at Lawrence Berkeley Nation Laboratory.	2
1.3	A system diagram of the Keck Telescope active control for a segment.	3
1.4	A figure of the GMT pupil and the initial plan to phase the mirrors[1].	3
1.5	A figure of the spot layout for the Keck phasing camera [4].	4
1.6	A conceptual drawing of how a vector apodizing phase plate works [3].	4
1.7	Figure showing how adding an asymmetry to the pupil plane propagates even phase aberrations and not through a symmetric pupil plane [3].	5
2.1	Asymmetric pupil planes used for simulation of the GMT FPWFS test	7
2.2	Isolated segment manipulation	8
2.3	Pupil and Focal plane of tilt applied to segment 4.	9
2.4	Focal plane response for tilt on segment 4.	10
2.5	A visual of Singular Value Decomposition	10
2.6	Singular Values of the Control Matrix	11
3.1	Paraxial view of the GMT testbed	13
3.2	Shear plate interferometer examples.	14
3.3	Example of how to read a shear plate interferometer [9]	15
3.4	Focal plane images	15
3.5	An overexposed vAPP image taken on our optical setup. The image was overexposed to show all the features. From here, further images were underexposed.	16
3.6	17
3.7	Showing noll indexing compared to a visual of the Zernike mode basis set.	18
4.1	Plots of each segments correlation between input aberration amplitudes and the output. There are 21 lines for each mode in the modal basis set.	19
4.2	Zoom in of Figure 4.1 to show linear region in tilt response.	20
4.3	21
A.1	All 21 response images. Columns are Piston, Tip, and Tilt and rows are segment number.	24
B.1	Piston correlation between -30 to 30 nm.	25
B.2	Tip correlation between -30 to 30 nm.	25
B.3	Tilt correlation between -30 to 30 nm.	26

List of Tables

List of Abbreviations

GMT	Giant Magellan Telescope
PSF	Point Spread Function
DM	Deformable Mirror
WFS	WaveFront Sensor
FPWFS	Focal Plane Wavefront Sensing
vAPP	Vector Appodizing Phase Plate
RM	Response Matrix
CM	Control Matrix
A#	Achromat number

Dedicated to my friends and family who helped keep me going.

Chapter 1

Introduction

Contents:

1.1	Segmented Mirrors / Active Optics	2
1.2	FPWFS	4
1.2.1	Vector Apodizing Phase Plate	4
1.2.2	Asymmetric Pupil	5

Advances in astronomy come in many forms, from the exploration of new theories to new observational techniques. But astronomy would not be possible without the main tool of the astronomer, the telescope. Starting from when Galileo Galilei first pointed his telescope to the night sky, astronomers have been demanding more from their telescopes. The only way to enhance a telescopes resolving power is to increase the primary aperture of the telescope. In the early 1900's telescopes were made up of a large single optics for the primary aperture. However, there is a limit to how large you can make a single optic.

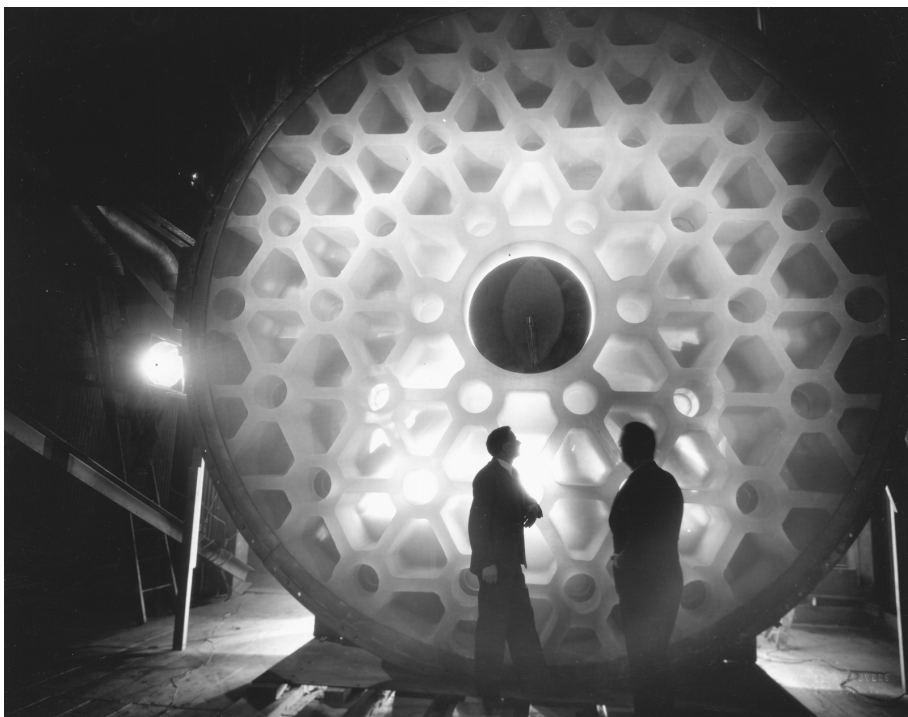


FIGURE 1.1: Image of the Hale 200-inch (5.1m) primary mirror. The honeycomb structure was to reduce the mass of the optic and make the surface more ridged

Eventually, these mirrors were becoming so large that the mirrors would sag under their own weight. These large optics quickly became heavier and needed more mechanical supports. In order to solve this problem, a honeycomb substructure was designed to keep the mirrors lighter and more ridged. Figure 1.1 shows the primary mirror of the 200-inch Hale telescope and backlight to show the structure. While this helped keep large single optics rigid, there is still a limit to how large one optic can be. The University of Arizona's Large Optics Facility is capable of constructing 8.4 meter mirrors [6]. One of the reasons for this limit is that this is roughly the maximum width of bridge underpasses in Arizona. In order to achieve larger primary apertures, a different approach is needed.

1.1 Segmented Mirrors / Active Optics

In 1977, Dr. Jerry Nelson along with Dr. Terry Mast and a team of scientists at the Lawrence Berkeley National Laboratory, were tasked with designing a 10-meter telescope [2]. The design they came up with was to use 36, 1.8 meter, hexagonal segments combined to make a 10-meter aperture (Figure 1.2). In order to make this work, all the segments needed to be aligned to sub-wavelength position. This was accomplished by what is known as active optics.

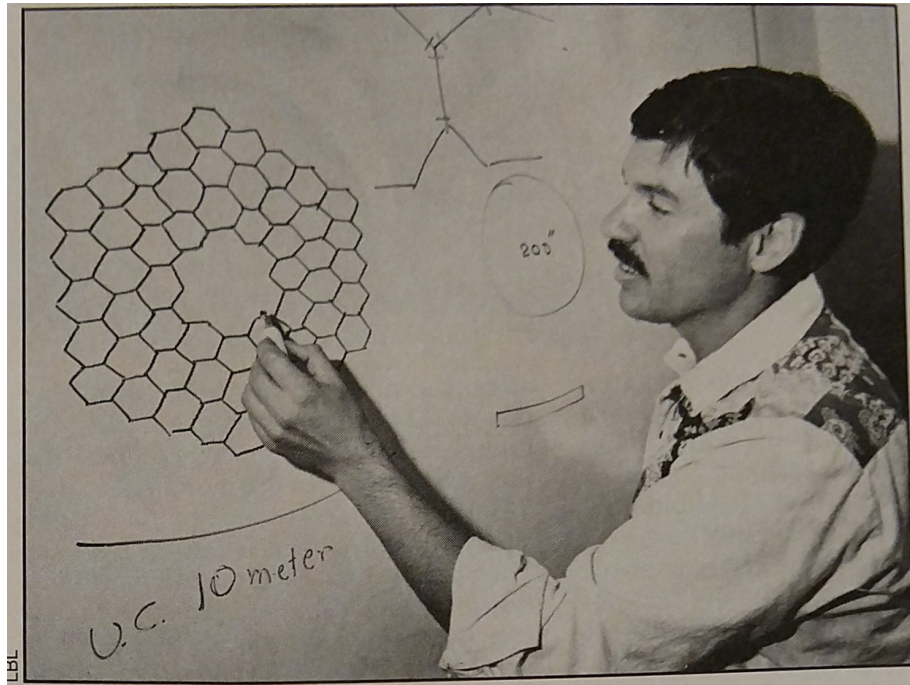


FIGURE 1.2: Jerry Nelson showing his segmented mirror design at Lawrence Berkeley Nation Laboratory.

Active optics is the active control of each mirror segment so that all segments act as one large optic. This is accomplished with nanometer level precision and differential capacitors to measure relative segment movement [7]. This system is continuously running during observation and makes corrections from vibrations that the telescope may experience (i.e mechanical vibration, wind shake, etc). The Keck position sensors are accurate to $\approx 30\text{nm}$ using differential capacitors. A system view of the the Keck active optics can be seen in Figure 1.3.

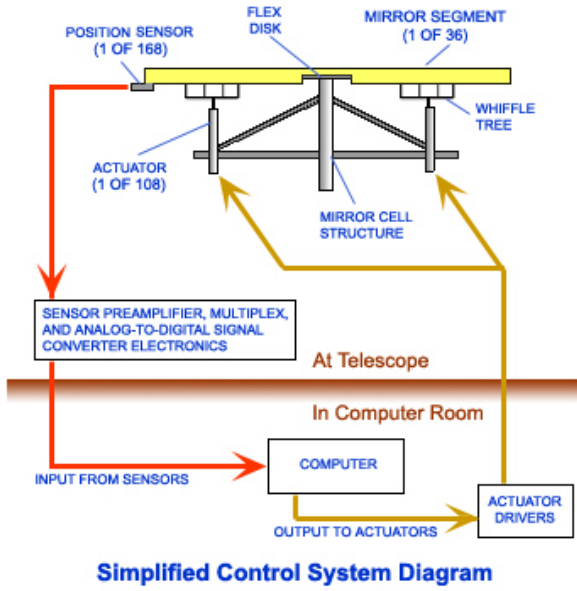


FIGURE 1.3: A system diagram of the Keck Telescope active control for a segment.

Instead of hexagonal segments the Giant Magellan Telescope will be using seven, 8.4-meter, circular segments to make up its 25 meter aperture (Figure 1.4). Figure 1.4 shows the initial plan to phase the GMT segments using laser interferometers to detect displacements for both fine and coarse motions [1]. However, these position sensors, like the capacitors, are differential and need to be calibrated. Typically, a phasing camera with a wavefront sensor is used to phase the mirror segments together.

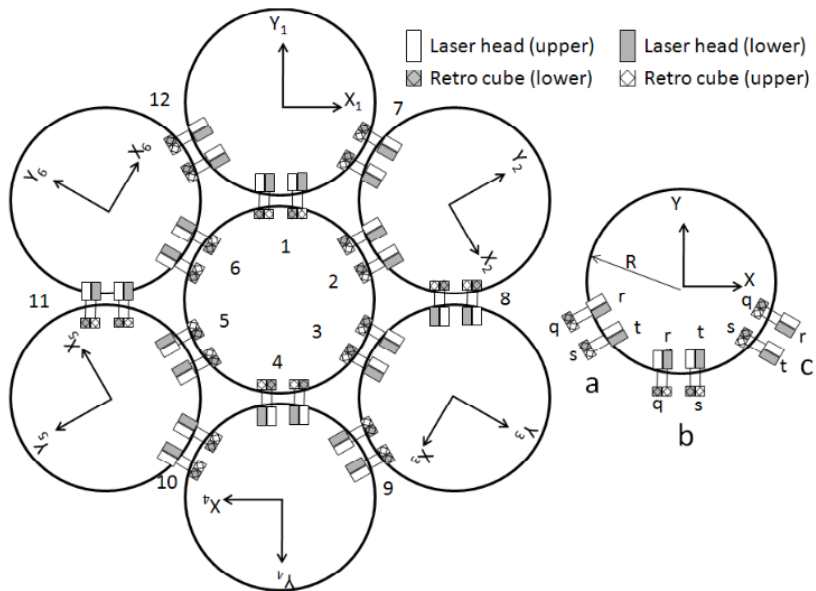


FIGURE 1.4: A figure of the GMT pupil and the initial plan to phase the mirrors[1].

For example, the case of the Keck telescope, there is a separate instrument all together mounted on a bent Cassegrain port [4]. This camera uses a Shack-Hartmann

Wavefront sensor to measure the piston, tip, and tilt of each segment (Figure 1.5). However, for high contrast imaging, this is not an accurate enough way to phase the mirror segments. High contrast imaging requires as little error as possible in all of the optical systems and the ability to ensure that segments are phased at the focal plane of the camera is highly desirable. The process of detecting wavefront aberrations in the science images is called Focal Plane Wavefront Sensing (FPWFS).

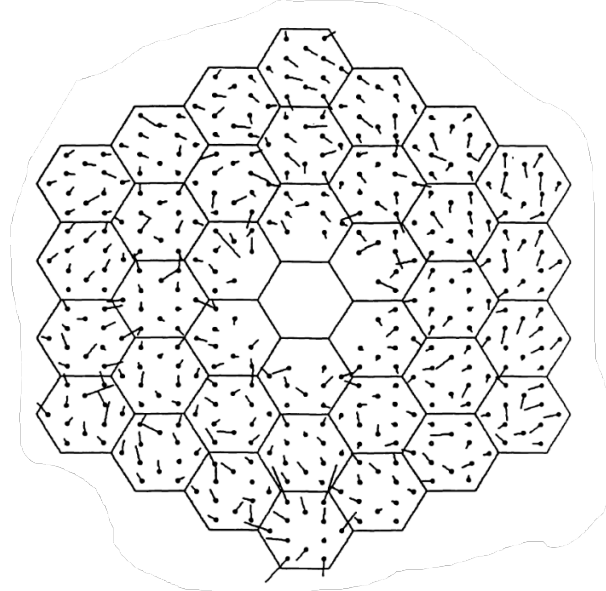


FIGURE 1.5: A figure of the spot layout for the Keck phasing camera [4].

1.2 FPWFS

1.2.1 Vector Apodizing Phase Plate

There are a few different approaches to doing FPWFS, but for this paper we will focus on using a type of coronagraphic imaging optic called a vector apodizing phase plate (vAPP). A vAPP is a half-wave retarder placed in the pupil-plane. The apodizing phase plate portion of the optic separates the right and left handed circular polarization of light and then spatially separated by a phase ramp (Figure 1.7) [3].

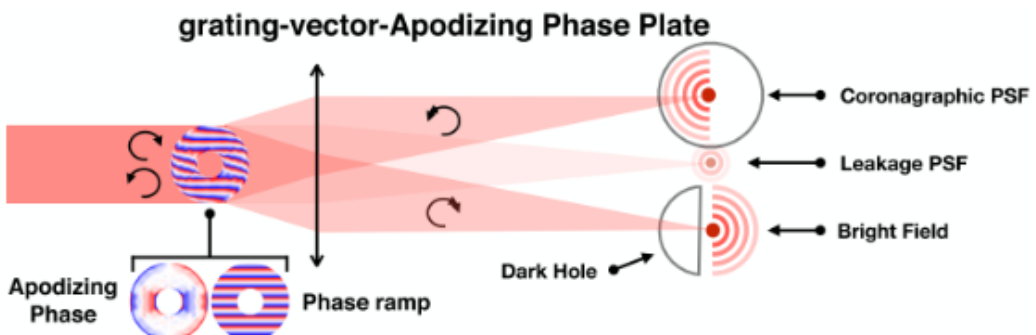


FIGURE 1.6: A conceptual drawing of how a vector apodizing phase plate works [3].

The spatial separation after being focused will show in the focal plane as two separate coronagraphic PSF's. However, the portion of the light that is not polarized will pass through the vAPP unaffected and will show in the focal plane as a standard PSF that can be used for referencing. But for the purposes of this thesis, we will be looking at the three PSFs and use them to deconstruct phase differences in the segments of the GMT.

1.2.2 Asymmetric Pupil

Work and theory done in this section is referenced from Steven Bos's paper *Focal-plane wavefront sensing with the vector Apodizing Phase Plate* [3].

What makes wavefront sensing possible with a vAPP is the asymmetry that is placed in the pupil plane. The electric field in the pupil can be written down as:

$$E_{\text{pupil}}(r) = A(r)e^{i\theta(r)} \quad (1.1)$$

$$= A(r)(\cos[\theta(r)] + i \sin[\theta(r)]) \quad (1.2)$$

As seen in Equation 1.2, there is an imaginary component to the electric field. Propagate this to the focal plane, we get a similar equation only with an added constant of integration. So this means that only some of the aberrations will appear in our focal plane. Specifically even phase aberrations will be left out of the focal plane while odd phase aberrations will continue to pass through. Adding an asymmetry to the pupil plane creates an odd amplitude which generates a real electric field. The real electric field will interfere with the aberrations' real electric field and will enable detection of the aberration in the focal plane [3].

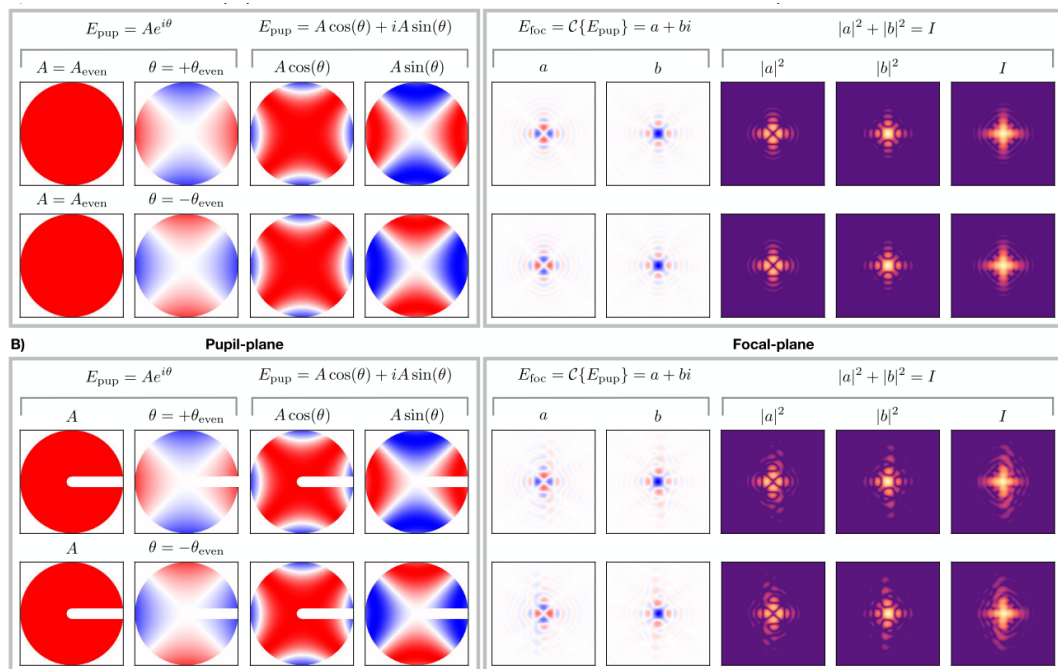


FIGURE 1.7: Figure showing how adding an asymmetry to the pupil plane propagates even phase aberrations and not through a symmetric pupil plane [3].

Chapter 2

Simulation

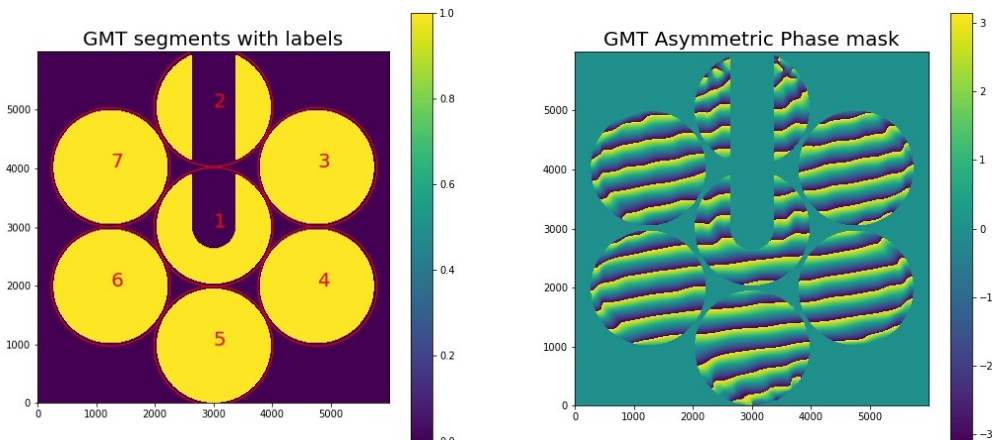
Contents:

2.1 Response Matrix	7
2.2 Control Matrix	10

The simulation portion of this research was to find what the response in the focal plane of our science image would be if one or more of the segments was out of phase from the rest. In order to do this, one segment will be isolated at a time and each of the three aberrations will be applied to it (Piston, Tip, or Tilt). All 21 combinations for P/T/T for all seven segments will be put into a matrix called the response matrix (RM). All coding was done in python using the python package HCIpy made in house at Leiden University [[por2018hcipy](#)]. This section will go into the process of building the response matrix as well as preparing the FPWFS.

2.1 Response Matrix

At the beginning of this project I was given two files, both of which were representative of the GMT pupil. One was a binary amplitude mask of the GMT pupil (Figure 2.1a) and the other was the phase mask (Figure 2.1b) that would be induced by the vAPP. Both masks have the asymmetry discussed in §1.2.1 in order to detect all of the modal basis set in the focal plane.



(A) Amplitude mask of the GMT pupil. Each segment is labeled 1-7 for which segment is to be iso-vAPP. (B) GMT phase mask that will be induced by the code. Each segment has a sinusoidal wave going across each segment.

FIGURE 2.1: Asymmetric pupil planes used for simulation of the GMT FPWFS test

In order to apply aberrations to a segment, I needed to isolate one of the segments. The code makes a circle of ones roughly the shape of the segment, and zeros across the rest of the array. When the circle mask was multiplied by Figure 2.1a we get the segment isolated (Figure 2.2a). With the segment isolated, we now want to add an aberration to this segment. As an example I will look at tilt. With the segment isolated, the code generates a tilt across the entire image and then makes sure that the values range from -1 to 1 only for the segment (Figure 2.2b).

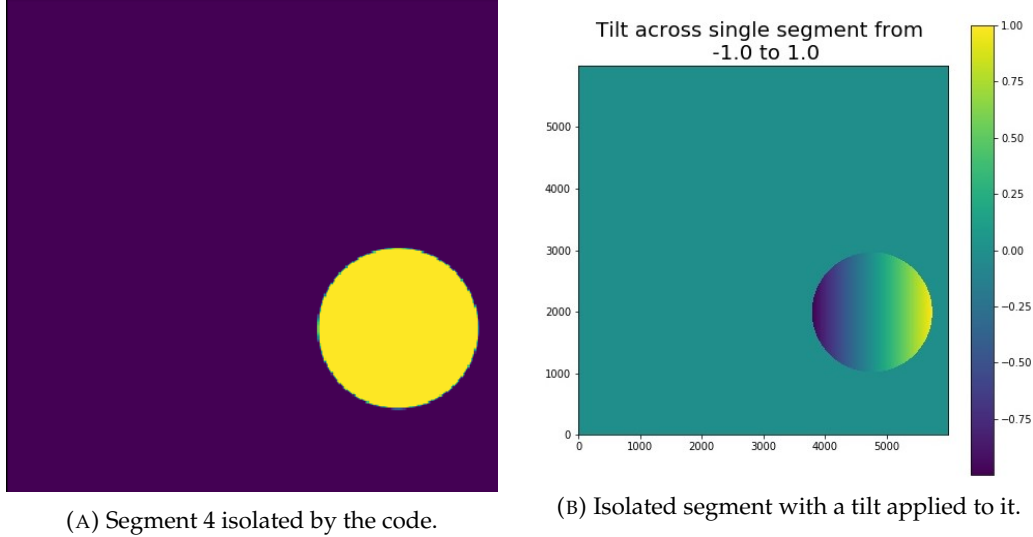


FIGURE 2.2: Isolated segment manipulation

However, we want to know the physical values of the tilt rather than just applying a tilt to the segment. In order to do this, we will apply an optical path difference (OPD) between the unaberrated segment and the segment with aberration. The phase difference is given by:

$$\phi = 2\pi \times \frac{d}{\lambda} \quad (2.1)$$

Where d is a distance in nanometers and λ is the operation wavelength. In this case, $\lambda = 532\text{nm}$. This is because the vAPP used on our optical testbed was tuned for lasers operating at 532nm. For simplicity, the code constructed the matrix for an OPD of 1nm so Equation 2.1 is simplified to $\phi = 2\pi/\lambda$. With the phase difference calculated, it is multiplied by the tilt array (Figure 2.2b), to give us a segment with the appropriate values. With the modification done to the segment, next step is to recombine the aberration (Figure 2.2b), amplitude mask (Figure 2.1a, as well as the phase mask (Figure 2.1b). To do this, I used the following equation:

$$I = A \times e^{i\phi} \quad (2.2)$$

Where I is intensity, A is the amplitude (Figure 2.1a) and ϕ is the phase of light (Figure 2.1b). However, just using Equation 2.2 will give a unaberrated image. Using the OPD, we combine the aberration and unaberrated pupil plane in the exponential because these are phase differences. This is done for each of the three PSFs that come from the vAPP. So we now have three different intensity equations:

$$I_{top} = A \times e^{(i \cdot (\phi_{ab} + \phi))} \quad (2.3)$$

$$I_{leakage} = A \times 0.1 \times e^{i\phi_{ab}} \quad (2.4)$$

$$I_{bottom} = A \times e^{(-i\phi) + (i\phi_{ab})} \quad (2.5)$$

Here ϕ_{ab} is the phase aberration we previously made, and the multiplication factor of 0.1 for Equation 2.4 is an intensity approximation of the leakage term. With all of these combined we get a pupil plane as shown in Figure 2.3a. However, we want to propagate each PSF separately and then add up the intensities. Propagation is done with an inbuilt function of HCipy called `FraunhoferPropagator [por2018hcipy]`. After each PSF is propagated and added together in the focal plane, we get an image like that in Figure 2.3b.

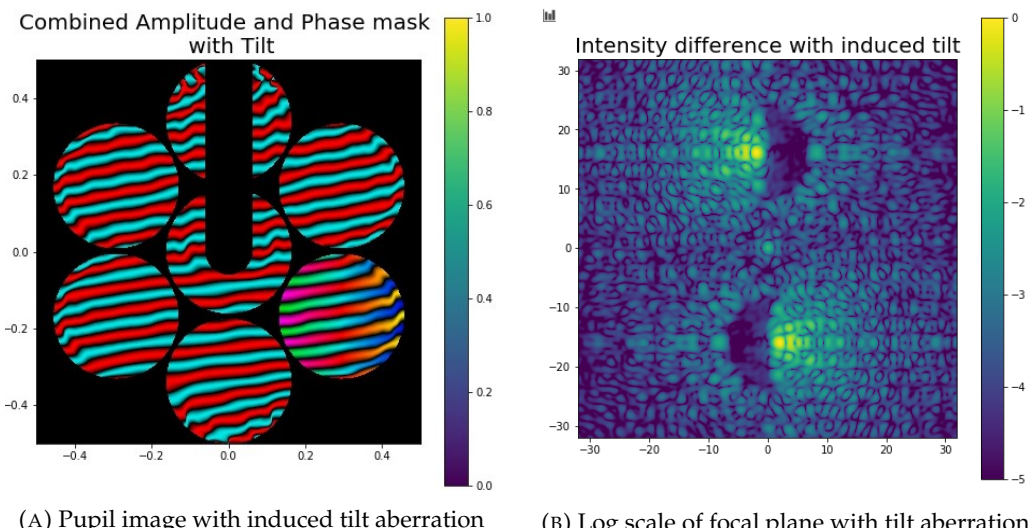


FIGURE 2.3: Pupil and Focal plane of tilt applied to segment 4.

Last step is to find the response in the focal plane for this aberration. This is simply done by repeating this process but instead changing Equation 2.1 to have a negative OPD applied to it. So the equation now becomes $\phi = -2\pi/\lambda$. After repeating the process, we get a new focal plane image. Now the response for a tilt on segment 4 can be calculated by taking $I_{pos} - I_{neg}$ (Figure 2.4). This image is stored as a 1-D vector and all 21 combinations of P/T/T for each of the seven segments are stored in a matrix. This is our Response Matrix. Now that there is a RM, we want to create the inverse of this matrix so that an inputted aberration can output an amplitude of each mode in our modal basis set (P/T/T). For a full array of response matrix images please refer to Appendix A.

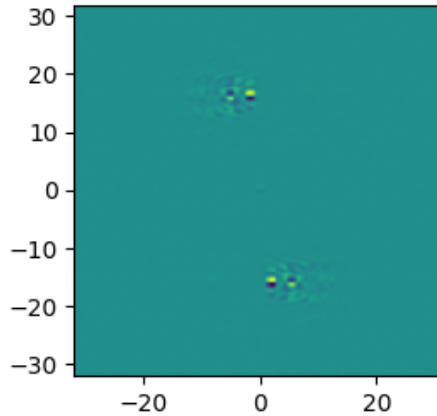


FIGURE 2.4: Focal plane response for tilt on segment 4.

2.2 Control Matrix

Construction of the control matrix involves taking a pseudo-inverse of the RM. This is done using singular value decomposition of the RM. Singular value decomposition (SVD) in linear algebra, is a way of decomposing a real or complex square matrix into the pseudoinverse of a matrix [5]. First we decompose our response matrix M into $M = U\Sigma V^*$ and the pseudoinverse is:

$$M^\dagger = V\Sigma^\dagger U^* \quad (2.6)$$

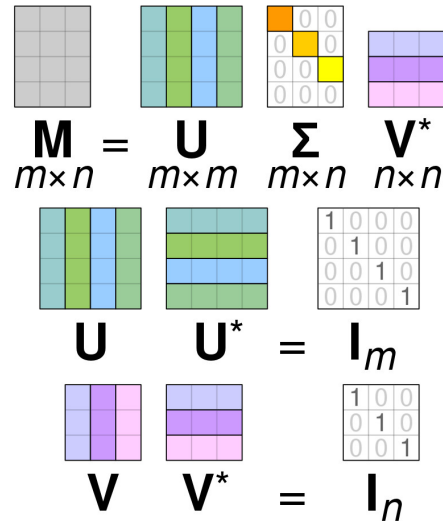


FIGURE 2.5: A visual of Singular Value Decomposition

Where Σ^\dagger is the pseudoinverse of Σ . This is formed by replacing every non-zero diagonal entry by its reciprocal and transposing the resulting matrix [5]. A visual example of this process can be seen in Figure 2.5. Luckily all this complicated matrix inversion is simply done in HClipy using the function `inverse_tikhonov` [`por2018hcipy`]. However, to test the inversion of the matrix, I plotted the singular values Σ and compared them to previous values calculated (Figure 2.6).

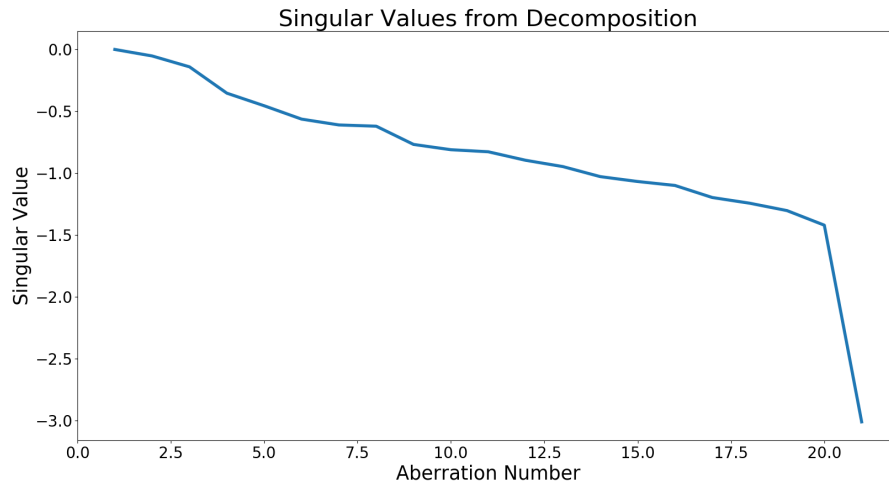


FIGURE 2.6: Singular Values of the Control Matrix

The singular values were confirmed to match previous versions of other response matrices made for the GMT. Therefore, we could move on to testing the wavefront sensing ability of our system. To test this, we first take a reference image of an unaberrated focal plane and subtract that from an aberrated image. The left over image is a residual intensity between the two images. With that image, we can take the dot product of the control matrix and the residual image to get the amplitudes of all the modal basis set. The results of this will be discussed in Chapter 4. Now that we have shown that we can do focal plane wavefront sensing with a vAPP, we can go on to physically demonstrating it.

Chapter 3

Optical Testbed

Contents:

3.1 Optical Layout	13
3.2 Optical Alignment	14
3.3 Images & Wavefront Decomposition	16

With the simulation work done showing that we can indeed do focal plane wavefront sensing on the GMT pupil with a vAPP, we now must show that we can do FPWFS on the optical bench.

3.1 Optical Layout

The goals of the optical testbed were to simulate piston, tip, and tilt onto each segment of the GMT pupil using a deformable mirror (DM). So the constraints of our optical system were to match the size of the DM and then zoom onto the GMT vAPP. First step was to couple a 532nm laser to a single mode optical fiber. As the laser light leaves the fiber, it will diverge. The light is collimated using an achromat onto an 11mm circular aperture. The aperture size was dependant on the aperture size of the DM and made slightly undersized in order to avoid the DM edge actuators which tend to not perform reliably. With the entrance pupil (EP) set, the achromats need to have a 1:1 relay of the pupil plane onto the DM. Therefore they were all set to the same focal length.

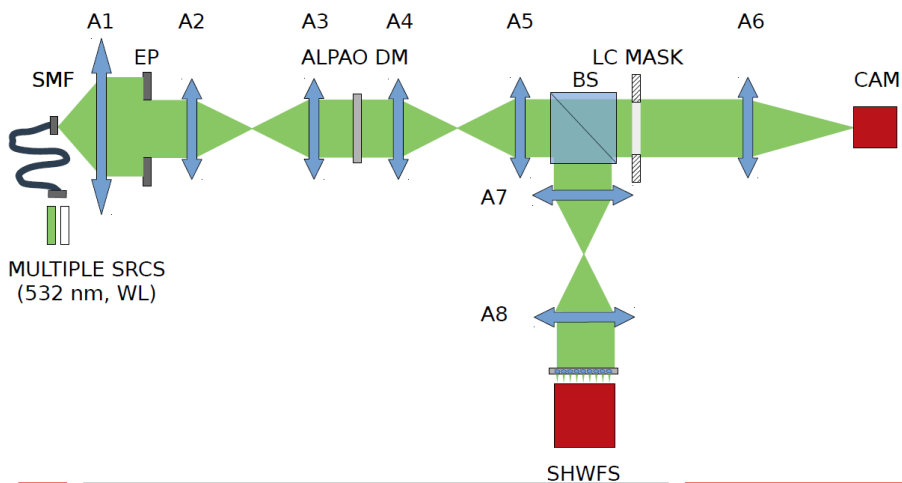
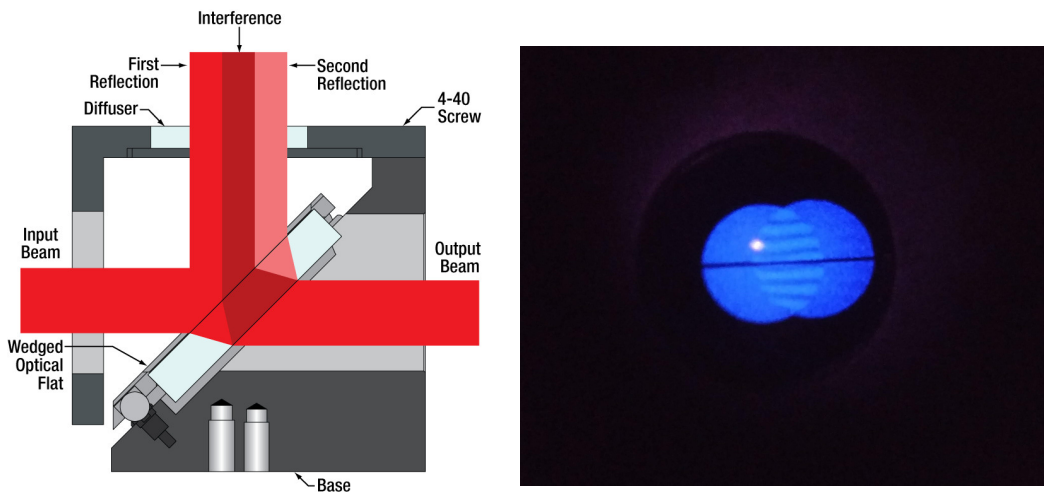


FIGURE 3.1: Paraxial view of the GMT testbed

After the DM, there needed to be a $\approx 1:2$ relay in order to zoom the pupil from the 11mm DM aperture to the $\approx 6\text{mm}$ vAPP aperture on the LC Mask. Then from the vAPP, the last achromat needed to have a long enough focal length to Nyquist sample the Airy core of the PSF. Before the LC MASK, a beam splitter was put in to direct light to a Shack-Hartmann wavefront sensor. This was so that verification of the aberrated wavefront was possible. The decision to use achromats rather than monochromatic lenses was made so that other projects could use other wavelengths for their purposes. However, our vAPP was tuned to 532nm. Figure 3.1 shows a paraxial design of the described layout. However, due to technical difficulties and with the addition of the current pandemic, the DM was replaced by a simple fold mirror.

3.2 Optical Alignment

Because the purpose of the optical bench was to do wavefront measurements, optical aberrations were to be kept to a minimum. This meant going through a rigorous alignment procedure. Initially we set up the optical bench to a rough approximation of the focal distances to get the total size of the layout. Then each optic position was marked and removed. A few Iris's was mounted to a post and measured the height of the outgoing light from the fiber optic. This was so that we could keep a continuous height through out the entire system. Next first achromat (A1) was put back in the system. In order to properly collimate the light path, we used a shear plate interferometer. How a shear plate interferometer works, is that as light passes through a 45 degree angle window, part of the light is reflected on each surface. A diagram of this can be seen in Figure 3.2a.



(A) Diagram of how a shear plate interferometer works [9]. (B) Fringe pattern of the shear plate interferometer.

FIGURE 3.2: Shear plate interferometer examples.

The first reflection interferes with the second reflection to cause an interference pattern like the one in Figure 3.2b. When the fringe pattern is at a tilt, then the beam is either converging or diverging (Figure 3.3). It is also possible to view other aberrations with a shear plate interferometer. As seen in Figure 3.2b, the lines have a slight curve on the left hand side of the window. This could possibly mean that there is

some spherical aberrations in our system. All of the achromats are spherical optics so this is something we can only try to minimize and then move on.

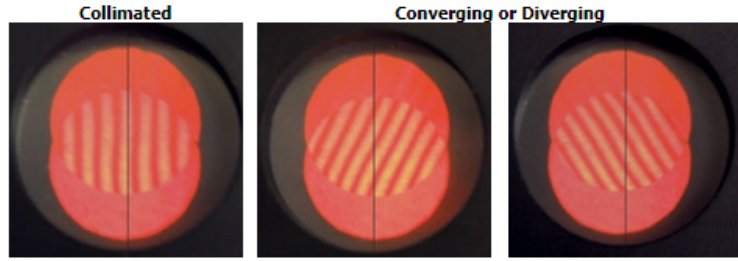


FIGURE 3.3: Example of how to read a shear plate interferometer [9]

With the beam collimated, the reference iris was placed in the system to ensure that the height of the beam had not changed. Next was to do a near/far test with the iris. The near/far test can be used to approximate collimation, however we used this test to make sure that the light path was always pointing straight and not diverting light off at an angle. When we were satisfied that the light was properly collimated and pointing correctly, the entrance pupil was mounted. It was essential that the entrance pupil be at the center of the light column as well. Laser light leaving the fiber is not equally illuminated across the pupil, so if the entrance pupil was not concentric with the light column, then that could lead to additional aberrations.

Next was to refocus the light. In order to test the focal plane a test camera was placed at the focus. In most cases, we could simply look at the airy rings and core to determine what aberrations we are seeing. However, the first focal plane was too fast and we were unable to properly sample the PSF. What we were able to do was put the camera before the focal plane and move it through and past the focal plane. This would show if there were any signs of coma or astigmatism. This same process for collimation and focus alignment was repeated for the rest of the system.

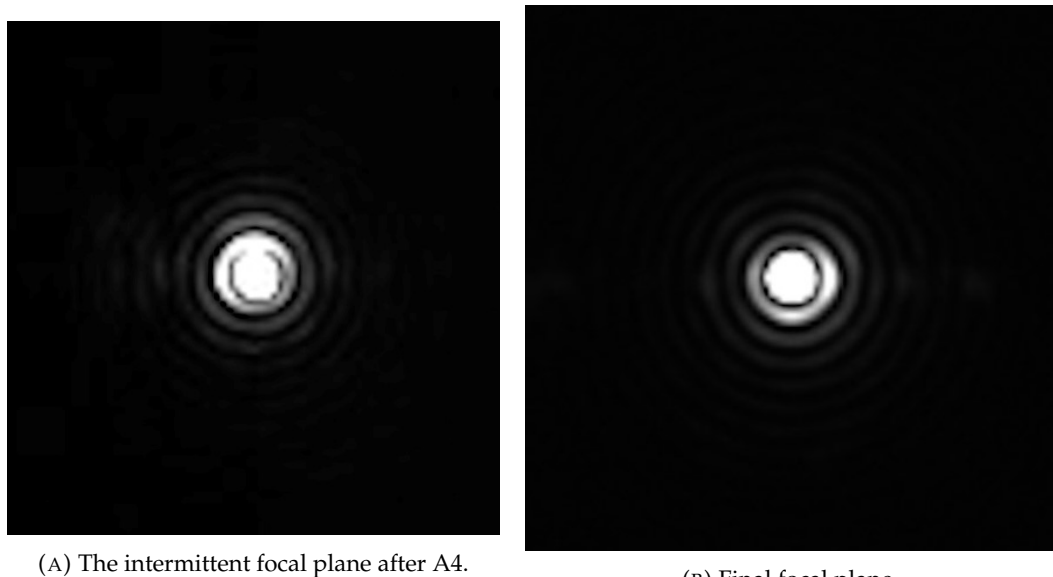


FIGURE 3.4: Focal plane images

For the flat mirror we put in place of the DM, we needed to divert the light as little as possible to limit the tilt aberration in the system. After we placed this

pseudo-DM, we double checked the aiming and collimation using the reference iris's and shear plate interferometer. Then a second mirror was placed to continue the light path down the reference holes in the breadboard.

After collimation, A4 was placed in. A4 was a long enough focal length in order to zoom from the 11mm DM aperture to the \approx 6mm aperture that we were able to properly sample the Airy rings. The intermittent focal plane can be seen in Figure 3.4a. This allowed for tighter alignment of A4, however as you can see in the figure, there is a slight coma. This is most likely due to small misalignments in A2 that we could not properly measure. From here the rest of the system was set up in the same way. We continued the system without injecting the vAPP so that we could see the optical quality of our final focal plane. The final result can be seen in Figure 3.4b. Then the last step was to inject the vAPP into our system into the pupil plane after A5. After proper alignment we arrived at the final coronagraph image (Figure 3.5). Now that the system is capable of taking coronagraphic images, we need to prove that the system can do wavefront sensing.

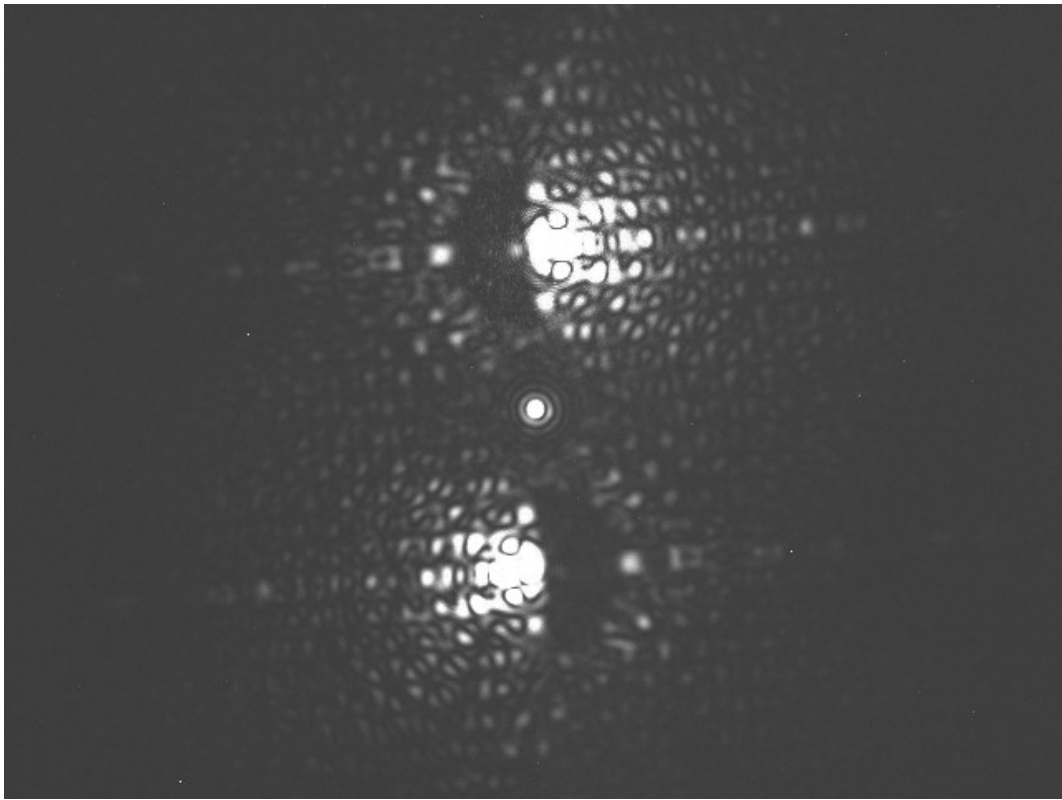
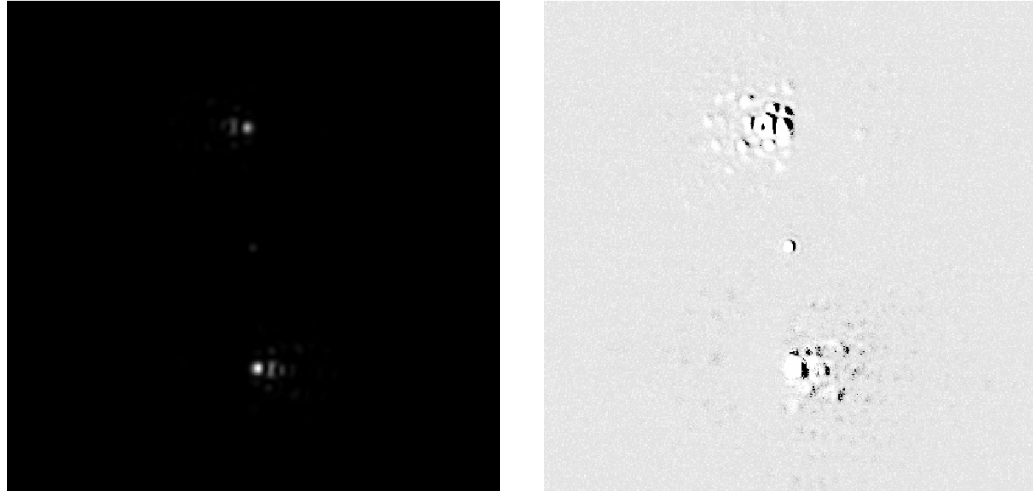


FIGURE 3.5: An overexposed vAPP image taken on our optical setup. The image was overexposed to show all the features. From here, further images were underexposed.

3.3 Images & Wavefront Decomposition

Once, we could take images of the vAPP, a series of exposures were taken and background subtracted by taking a series of dark exposures and taking the median of those images. Due to the unfortunate issues with the DM, we opted to show that the system could do wavefront sensing using a different approach. The PhD student and one of my advisors Steven Bos, wrote a code to do focal plane wavefront sensing of vAPP images. First step is to take the exposed image and turn the rectangular

array and make it square with the leakage term in the middle (Figure 3.6a). The code then needs approximate locations of the three PSFs in radians. This is easily found by plotting the image in HCipy and marking the x and y locations of the three PSFs. There are other parameters that the code needs such as tilt of the PSF and wavelength. Tilt can be seen in the overexposed image (Figure 3.5), and can be calculated using ds9.



(A) An under exposed vAPP image like that of Figure 3.5 cropped to a square
(B) Residuals of the simulated image to match input image (Figure 3.6a).

FIGURE 3.6

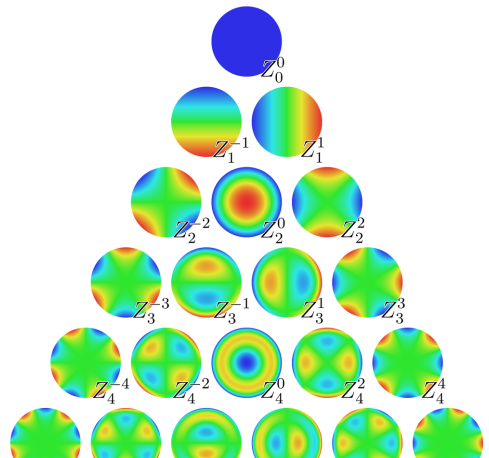
Next the code takes these inputs and the same amplitude and phase masks used in Chapter 2 to generate an unaberrated vAPP focal plane. However, in order to match the optical bench, the amplitude mask was replaced by a circular aperture rather than the GMT pupil. With this in place, a few runs of the code were necessary to match the PSFs using small variations in the wavelength to control the spread of the three PSFs. With the simulated vAPP image made, the code then goes through a series of Noll index Zernike modes. Noll index is a way of ordering the zernike modes using one index Z_j rather than two variables $Z_n^{m'}$ [8]. The indexing of the Noll sequential indicies is as follows:

$$j = \frac{n(n+1)}{2} + |m'| + \dots \quad (3.1)$$

A comparison of the Noll index set and the Zernike mode ordering can be seen in Figure 3.7. The code ignores the first four indices of the Noll basis (piston, tip, tilt, and defocus) because the system is not sensitive to these modes. To be clear, the system is insensitive to global piston, tip, and tilt. However, we are looking for piston, tip, and tilt of individual segments which are detected by this process. Here the code takes the simulated vAPP image and propagates the image to the pupil plane and applies the first mode and changes the amplitude of that mode to best match the input image. This continues for each of the modes until the specified end mode. The output of this code is an amplitude of all the modal set and then summed into a wavefront image. The results will be discussed in §4.2.

n,m'	0,0	1,1	1,-1	2,0	2,-2	2,2	3,-1	3,1	3,-3	3,3
j	1	2	3	4	5	6	7	8	9	10
n,m'	4,0	4,2	4,-2	4,4	4,-4	5,1	5,-1	5,3	5,-3	5,5
j	11	12	13	14	15	16	17	18	19	20

(A) A table showing the Noll index ordering compared to the standard Zernike ordering[8].



(B) Zernike mode ordering [8]

FIGURE 3.7: Showing noll indexing compared to a visual of the Zernike mode basis set.

Chapter 4

Results

Contents:

4.1 Simulation Results	19
4.2 Testbed Results	21
4.3 Future Work	21

This chapter will go over the results of the simulation work as well as results from the optical testbed.

4.1 Simulation Results

With the control matrix in place, there needs to be data showing that there is a good linear correlation between the amplitude of the input wavefront aberration and what the system outputs. Going through the process used in §2.1, a new set of aberrations were made with a range of amplitudes. Then following the process described at the end of §2.2, we can compare the input amplitudes and what the code detects.

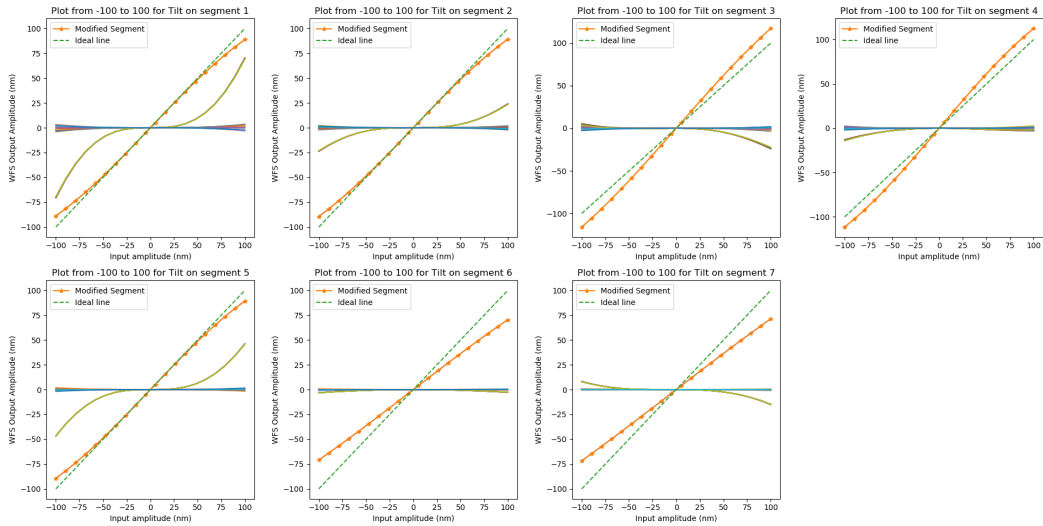


FIGURE 4.1: Plots of each segments correlation between input aberration amplitudes and the output. There are 21 lines for each mode in the modal basis set.

As an example we will focus on the tilt of each segment. As we can see in Figure 4.1, there is a linear region in the middle of each segment. There is also some response from other modes. This is cross-talk between other tilt modes from other

segments. However there is a region in the middle where cross-talk is limited. Therefore the code ran again at to see the where the linear region lies. In Figure 4.2, we can see there is limited cross-talk between the other modes and that there is a linear correlation between the input amplitude and the output amplitude.

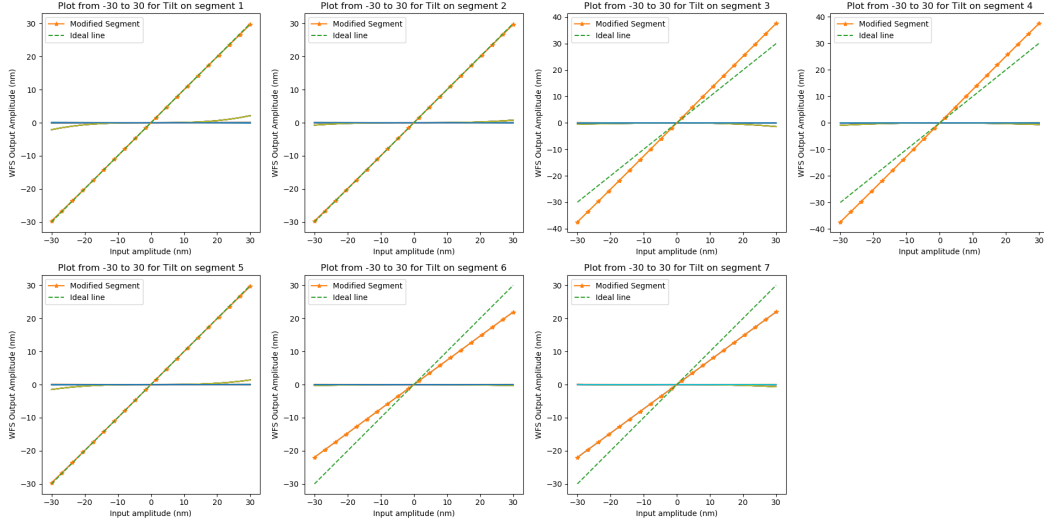


FIGURE 4.2: Zoom in of Figure 4.1 to show linear region in tilt response.

It should be noted that there is a slope difference on segments on segments 3, 4, 6, and 7. If we refer to Figure 2.1a, we can see that these segments are off axis and the aberration is perpendicular to the asymmetry. This is purely hypothetical but could warrant further investigation. However, these responses are still linear and can be corrected for. This slope offset only occurs when tilt is applied. All plots can be seen in Appendix B.

4.2 Testbed Results

After putting the exposed images through the code, the output is a wavefront error map and an output of each of the amplitudes of the modal basis set (Figure 4.3a). We can then make a plot of the amplitudes of each Noll index like that shown in Figure 4.3b. These aberrations were the aberrations we could not correct for in our alignment procedure. However, these plots show that our testbed demonstration can in fact do focal plane wavefront sensing.

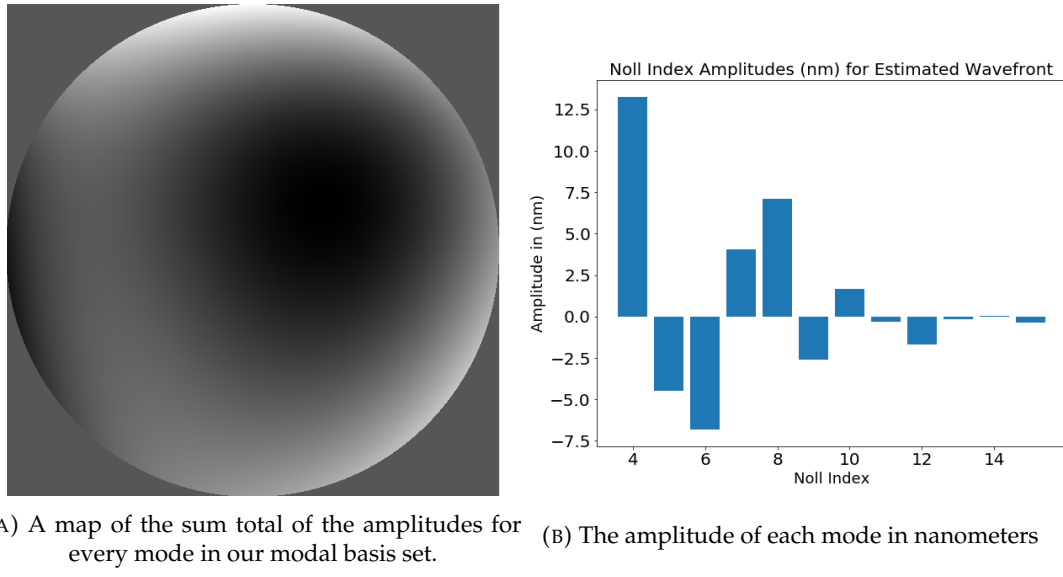


FIGURE 4.3

4.3 Future Work

The work done here shows that using an asymmetric pupil vector apodizing phase plate (APvAPP) can indeed do focal plane wavefront sensing. On top of that, simulation shows that we can use this process to phase the segments of the GMT. However, there is still more work that can be done. These images will be taken with a non-perfect detector. Images should have some Gaussian noise applied to them and see how the results differ. Some additional next steps are to create a closed loop control in simulation where a random set of aberrations are applied to the pupil and detected by the code. The code should then output the amplitude of the aberrations and correct for that. In addition, it would be good to demonstrate this on the optical testbed using a DM. The DM would be able to apply P/T/T to individual segments and then run a closed control loop to correct the aberrations on the DM.

Appendix A

Response Matrix Images

Image is quite large, go to next page.

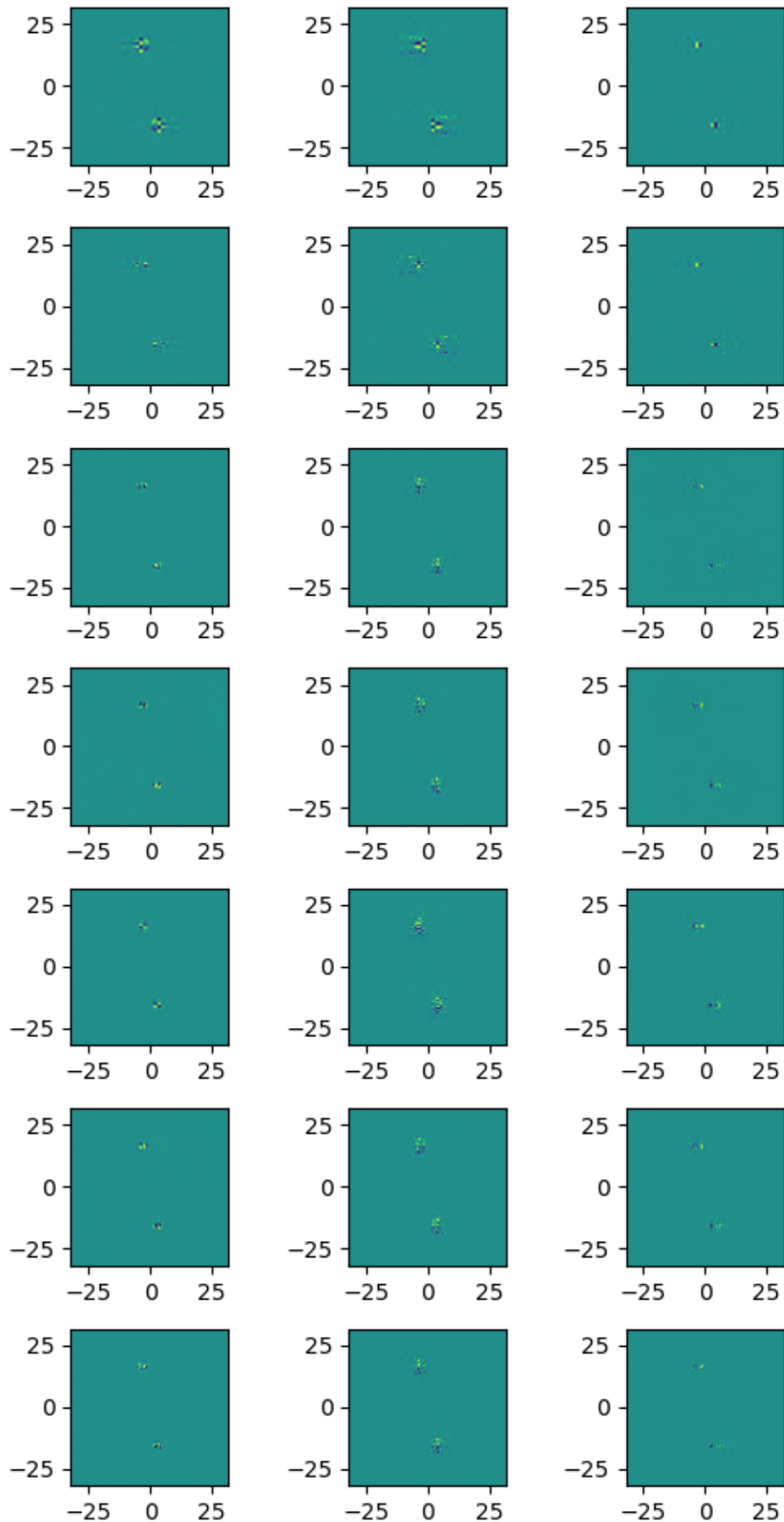


FIGURE A.1: All 21 response images. Columns are Piston, Tip, and Tilt and rows are segment number.

Appendix B

Simulation Results

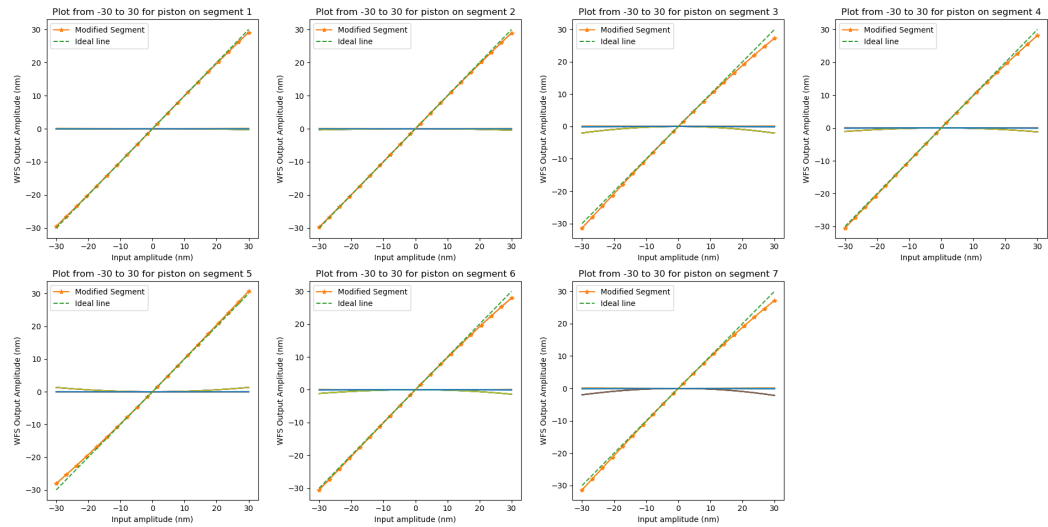


FIGURE B.1: Piston correlation between -30 to 30 nm.

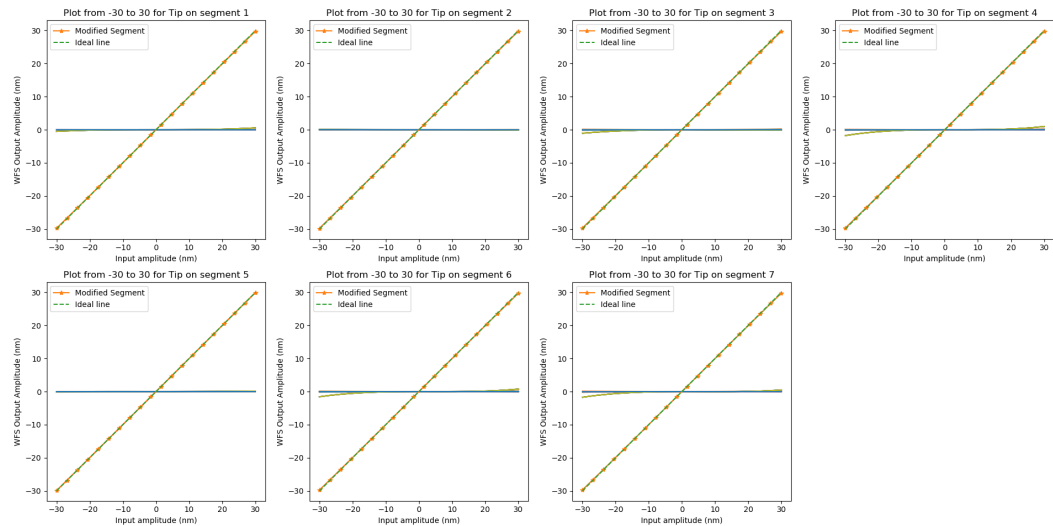


FIGURE B.2: Tip correlation between -30 to 30 nm.

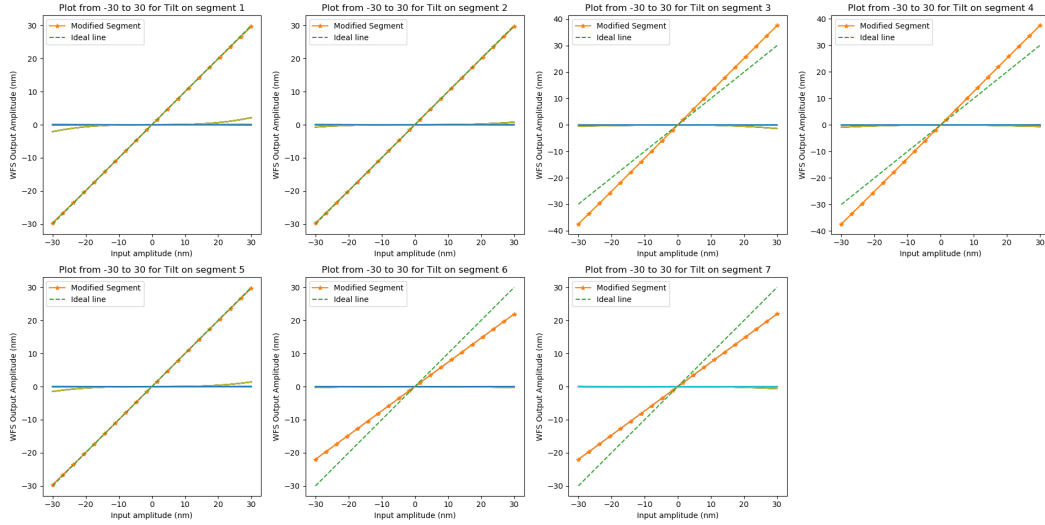


FIGURE B.3: Tilt correlation between -30 to 30 nm.

Bibliography

- [1] D Scott Acton and Antonin Bouchez. "Phasing metrology system for the GMT". In: *Ground-based and Airborne Telescopes IV*. Vol. 8444. 2012, p. 844423. ISBN: 9780819491459. DOI: [10.1117/12.925012](https://doi.org/10.1117/12.925012).
- [2] *Beating the Odds | W. M. Keck Observatory*. URL: https://web.archive.org/web/20101006071550/http://keckobservatory.org/cosmicmatters/article/beating_the_odds/.
- [3] S. P. Bos, D. S. Doelman, J. Lozi, O. Guyon, C. U. Keller, K. L. Miller, N. Jovanovic, F. Martinache, and F. Snik. "Focal-plane wavefront sensing with the vector-Apodizing Phase Plate". In: *Astronomy and Astrophysics* 632 (2019). ISSN: 14320746. DOI: [10.1051/0004-6361/201936062](https://doi.org/10.1051/0004-6361/201936062).
- [4] Gary A. Chanan, Jerry E. Nelson, Terry S. Mast, Peter L. Wizinowich, and Barbara A. Schaefer. "<title>W.M. Keck Telescope phasing camera system</title>". In: *Instrumentation in Astronomy VIII* 2198.June 1994 (1994), pp. 1139–1150. DOI: [10.1117/12.176697](https://doi.org/10.1117/12.176697).
- [5] Magnus R. Hestenes. "Inversion of Matrices by Biorthogonalization and Related Results". In: *Journal of the Society for Industrial and Applied Mathematics* 6.1 (Mar. 1958), pp. 51–90. ISSN: 0368-4245. DOI: [10.1137/0106005](https://doi.org/10.1137/0106005).
- [6] *LOFT, Large Optics Fabrication and Testing group with OEFF & RFCML | Developing advanced technologies for optical testing and fabrication of large optical components and systems*. URL: <http://www.loft.optics.arizona.edu/>.
- [7] Jerry E. Nelson and Terry S. Mast. "<title>Construction of the Keck Observatory</title>". In: *Advanced Technology Optical Telescopes IV* 1236.July 1990 (1990), pp. 47–55. DOI: [10.1117/12.19171](https://doi.org/10.1117/12.19171).
- [8] Robert J. Noll. "ZERNIKE POLYNOMIALS AND ATMOSPHERIC TURBULENCE." In: *J Opt Soc Am* 66.3 (1976), pp. 207–211. DOI: [10.1364/JOSA.66.000207](https://doi.org/10.1364/JOSA.66.000207).
- [9] *Shearing Interferometers*. URL: https://www.thorlabs.com/newgroupage9.cfm?objectgroup_id=2970.